Nuclear Instruments and Methods in Physics Research B68 (1992) 17–22
North-Holland

NIM B
Beam Interactions with Materials & Atoms

Laser cooling of stored ions in ASTRID: a storage ring for ions and electrons

J.S. Hangst [1], K. Berg-Sørensen, P.S. Jessen, M. Kristensen, K. Mølmer, J.S. Nielsen, O. Poulsen, J.P. Schiffer [2] and P. Shi

Institute for Physics and Astronomy, University of Aarhus, DK-8000 Aarhus C, Denmark
Søren Pape Møller Institute for Synchrotron Radiation, University of Aarhus, DK-8000 Aarhus C, Denmark

A small storage ring, ASTRID, for ions and electrons has been constructed. It is a dual-purpose machine, serving as a storage ring for either ions or electrons for synchrotron-radiation production. The ring has for more than one year been operational with ions and has recently been commissioned for electron storage. Both these running modes will be described as well as results given from the first experiments with laser cooled ions. Finally, prospects for experiments with superhigh mass and isotope selectivity will be discussed.

1. The facility

ASTRID was originally designed for storage of low-energy heavy ions for laser spectroscopic and laser cooling experiments and for atomic collision studies, most prominently recombination experiments. In the design phase of this heavy-ion machine it was realized that the requirements for ion operation could also fulfill design criteria for storing energetic electrons. Thus ASTRID could serve as a competitive VUV/XUV synchrotron-radiation source [1], in addition to a unique heavy ion storage capability.

The storage ring with injectors and associated laboratory space is located in an underground building in connection to the Institute of Physics, see fig. 1. The electron injector is placed in a separate well-shielded cave. There is no radiation shielding around the storage ring, and only during the brief periods of filling of the ring with electrons, the ring hall is evacuated.

1.1. The ion injector

Ions are preaccelerated in an isotope separator using a very stable (RMS < 1 V) 200 kV high-voltage supply. A variety of ion sources can be used with the separator to produce singly-charged ions of almost any type. A sputter ion source has also been used to produce negative ions. A charge exchange cell is installed after the separator magnet to facilitate the production of a wide range of negative ions. Differential pumping in the injection beamline separates the high-pressure ion source (10^{-2} Torr) from the storage ring vacuum (10^{-12} Torr).

1.2. The electron injector

A pulsed (10 Hz) race-track microtron [2] has been built to produce the 100 MeV electrons for the storage ring. The rf system is operating at 2998.6 MHz. The resonant energy gain is 5.3 MeV corresponding to 19 turns. Horizontal and vertical correctors are installed on every turn.

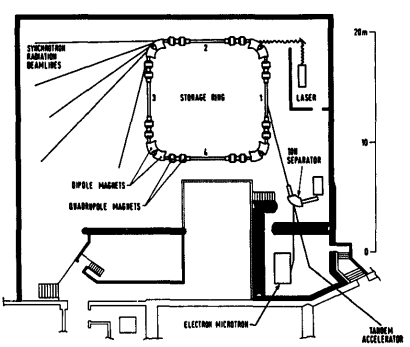

Fig. 1. Layout of the ASTRID laboratory.

[1] Also FNAL, ANL, and University of Chicago.
[2] Also ANL and University of Chicago.

Table 1
Parameters of ASTRID

General parameters of ASTRID	
Magnetic rigidity	1.87 Tm
Circumference	40 m
Tunes (hor, vert)	{2.29, 2.73}
Chromaticities (hor, vert)	{−3.4, −7.5}
Momentum compaction	0.053
Parameters of ASTRID for electron storage	
Nominal current	200 mA
Electron energy	560 MeV
Horizontal emittance	0.017 mm mrad
Critical energy, λ_c	330 V, 3.7 nm
Energy loss/turn	7.1 keV
Beam lifetime (Touschek)	24 h
Number of bunches	14
Rf system {frequency, amplitude}	{105 MHz, 25 kV}

1.3. The storage ring

The "ring" is a square, formed by four sets of 45° bending magnets, excited by a common coil. The quadrupoles are grouped in four families, so that the dispersion in two opposite straight sections can be varied continuously between 0 and 6 m without change of the tunes. Two families of eight sextupoles are available for chromaticity corrections. Superimposed on the air-cored sextupoles are eight horizontal and eight vertical correction dipoles. Furthermore, four horizontal correctors are available as back-leg windings on the main dipoles.

The vacuum system is designed for the 10^{-12} Torr region, as required for long storage times of the ions. Hence the system has been vacuum fired and is prepared for a 300°C in-situ bake-out. There is installed a total of 20 ion pumps and 24 sublimation pumps in the ring. Presently the system has only been baked to 150°C, resulting in an average pressure around 2×10^{-11} Torr, slightly lower than the pressures obtained in some of the early experiments.

Two different rf systems are used. For the ions, a ferrite-loaded cavity operating in the 0.4–5 MHz region yields a maximum voltage of 2 kV. For the electrons, a capacitively loaded coaxial TEM cavity operating at 104.9 MHz is used. This cavity was fabricated in steel, which was subsequently copper plated. A quality factor $Q \approx 8000$ is obtained.

Ions and electrons are injected with a magnetic septum (dc) and a kicker. For the ions an electrostatic kicker excited by a square pulse injects one turn. For the electrons, a magnetic kicker excited by a half-sine pulse is used to accumulate electrons. The septum is also designed for extraction of a high-energy electron beam. Clearing electrodes covering around half the circumference are installed in the ring to reduce ion-trapping effects. The kicker and rf-system is the only hardware being exchanged when swapping between electron and ion operation.

A variety of diagnostics is installed, including eight horizontal and vertical position pickups, scintillation screens, transverse and longitudinal Schottky pickups, beam-current transformer, beam scrapers and synchrotron-radiation detectors. A control system based on a NORD main computer with PCs as consoles is used.

2. The first electron run

The 100 MeV race-track microtron has been commissioned and routinely delivers 5–10 mA pulses of 1 μs width. A few turns are injected into the ring and captured by the 105 MHz rf system. About 0.3 mA has been captured in one shot, and several pulses have been accumulated to reach more than 100 mA. The electron beam has been accelerated to 500 MeV without significant losses. The decay of a stored electron beam at 500 MeV is shown in fig. 2. The lifetime is around 17 h at a pressure of 8×10^{-10} Torr. Only a modest rf power (1.5 kW) was fed into the cavity during these runs and no detectable outgassing of the vacuum system was observed. The pressure during electron operation is slightly higher due to the rf cavity for electrons.

The electron facility is presently being upgraded, including full power (20 kW) operation of the electron injector and better focusing in the injection beamline. To fully exploit the VUV/XUV synchrotron radiation, three experimental setups are added initially. An X-ray microscope has been finished and a plane grating monochromator (SX-700), operating in the 10–2300 eV range is operational, mainly for use in surface studies. Finally, a spherical grating monochromator for the 30–600 eV region is presently being constructed, mainly for use in atomic and molecular physics studies.

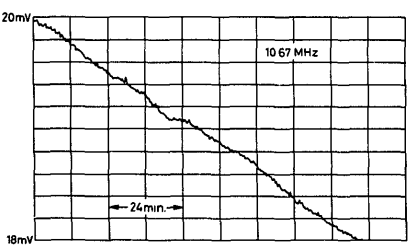

Fig. 2. Decay of a stored electron beam; the lifetime is 17 h.

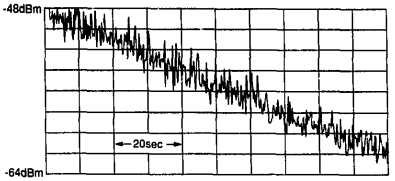

Fig. 3. Decay of an $^{166}Er^+$ beam; the lifetime is 30 s, limited by an average pressure of 2×10^{-11} Torr.

3. Ion runs

Since the startup of the facility many different ions have been stored in the ring. Long runs have been with $^{6,7}Li^+$ and $^{166}Er^+$ for laser-cooling experiments [3]. Other runs included simultaneous storage of $^{20}Ne^+$ and $^{40}Ar^+$ ions. Finally, a range of negative ions like F^-, Fe^-, OH^-, O^-, H^-, C^-, C_2^- and He^- has been stored. The ions were injected at energies in the range from 10 to 150 keV. The lifetime of the stored beam was limited by the vacuum, typically in the 10^{-11} Torr region, giving lifetimes of some seconds. In fig. 3 is shown the decay of an erbium beam as observed with a longitudinal Schottky pickup electrode. The observed closed-orbit deviations were less than 10 mm and could be corrected to less than 1 mm, limited by the position resolution, both horizontally and vertically by the correction magnets.

4. Laser cooling experiments

4.1. Introduction to laser cooling

Laser cooling [4] is the result of the velocity-selective transfer of photon momentum from a laser beam to a moving atom or ion. In the most basic laser cooling scheme, particles having a closed transition between two energy levels are utilized. Those particles which are in resonance with a laser beam absorb photons. Each photon transfers momentum of magnitude $h\nu/c$ to the absorbing particle, which recoils in the direction of the laser propagation. The photons are spontaneously re-emitted. The average momentum transfer from the re-emission vanishes due to symmetry. The net force is thus directed along the laser beam. The force is velocity selective because of the small width of the atomic transition, and velocity dependent through the Doppler effect. By tuning the frequencies of co- and counterpropagating lasers to accelerate slow particles and decelerate fast ones, one achieves cooling. The cooling limit, called the Doppler cooling limit, is given by $k_B T = 7h\Gamma/20$, where Γ is the homogeneous width of the cooling transition. Other schemes have been developed to cool particles to temperatures below the Doppler limit, but these will not concern us here (see ref. [5] for an overview of laser-cooling theory and experiment).

The use of lasers for cooling ions or atoms stored in traps is well documented [5]. More recently, it has become possible to cool energetic beams of ions circulating in storage rings. Unlike the trap experiments, which use up to six laser beams to cool all three spatial dimensions, storage ring laser cooling operates only on the longitudinal degree of freedom. In the first reported experiment, a beam of $^7Li^+$ ions with kinetic energy of 13 MeV was laser cooled to a longitudinal temperature of less than 3 K [6].

In addition to offering the potential for cooling to very low temperatures, the laser is a unique diagnostic tool. By measuring the laser-induced fluorescence (LIF) of a beam as a function of laser frequency, one can directly and nondestructively measure the velocity distribution of the circulating ions.

In the current set of experiments, we have used the storage ring ASTRID to investigate laser cooling and diagnostics of 100 keV $^7Li^+$ ions. We also discuss briefly recent experiments using $^{166}Er^+$. Finally, we comment on the implications of our experiments for the effort to achieve ordered or "crystalline" beams [7].

4.2. Apparatus for cooling experiments

The storage ring ASTRID and its associated optical experimental apparatus are shown schematically in fig. 4. The storage ring itself was presented in a previous

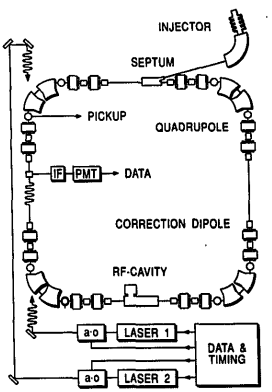

Fig. 4. Schematic of the ASTRID storage ring and associated laser apparatus.

section. We thus restrict the discussion to the associated optical equipment.

Windows at the ends of two straight sections allow laser light to pass into the vacuum chamber. Laser light is provided by two ring-dye lasers, which can be intensity modulated using acousto-optic modulators. Fluorescent light from the ions is monitored through an additional window which looks transversely at the beam. A telescope collects light and directs it to a photomultiplier tube (PMT). An interference filter (IF) of bandwidth 0.6 nm (FWHM) discriminates between fluorescent light (which is Doppler shifted relative to the direct laser light) and scattered light. The lithium experiments employed lasers and diagnostics in one straight section of the ring.

4.3. Experimental parameters

The 100 keV lithium ion beam utilized is actually a two-component beam. A fraction of the beam ($\sim 10^{-4}$) is produced in the metastable $1s2s^3S_1$ state; the remainder exists in the ground state. The metastable state is connected to the $1s2p^3P_2$ state by optical transitions, and is subject to laser cooling by virtue of a closed hyperfine transition ($F'' = \frac{5}{2} - F' = \frac{7}{2}$). The rest-frame wavelength of the transition is about 548.6 nm. The natural linewidth of the transition is $\Gamma = 3.7$ MHz, corresponding to a lifetime of 43 ns. The Doppler cooling limit is 88 μK. The branching ratio to the ground state is less than 10^{-5}.

After acceleration, the beam has a flattened velocity distribution. The initial longitudinal energy spread is ~ 1 eV, corresponding to $T \sim 100$ mK or $\delta p/p \sim 10^{-5}$. The initial transverse temperature is about 1000 K. Typical beam currents are ~ 10 μA, corresponding to roughly 10^9 particles injected. The average beam radius, measured by scanning a slit across the LIF image of the beam, was $r_{rms} \sim 3$ mm. This yields a particle density of about $10^6/cm^3$. The average pressure in the ring during these experiments was 3×10^{-11} Torr.

5. Laser diagnostics and beam relaxation

The laser has been used as a probe to monitor the longitudinal velocity distribution of the circulating beam. Fig. 5 shows the time development of the longitudinal temperature of the metastable lithium ions. In 30 μs the beam heats from ~ 100 mK to ~ 2 K. At this point the velocity distribution is measured to be thermal with a FWHM of 100 m/s. The temperature continues to increase up to ~ 200 ms after injection, which was the latest time measurable with our experimental setup.

This observed rapid longitudinal heating may be due to intrabeam Coulomb interactions. Such interactions can transfer momentum from the transverse degrees of freedom to the longitudinal one. The high transverse kinetic energy of the beam particles is a likely source of heating for a beam of the relatively high charge density found in ASTRID. To estimate the importance of this process, we have employed a binary collision description of intrabeam scattering due to Sørensen [8]. The model calculates the energy transfer rate from transverse to longitudinal motion for a beam with an initially anisotropic velocity distribution ($T_\perp \gg T_\parallel$). The measured beam size is first used to estimate the transverse energy of the beam. For ASTRID, the contribution of the space-charge force to the beam size is not negligible. The Sørensen description predicts an energy transfer rate of ~ 2 eV/s for the ASTRID beam at the time of injection. This is in good agreement with the initial slope of fig. 5, which gives 1.4 ± 1 eV/s. The shape of the curve in fig. 5 agrees qualitatively with the analytical predictions. A detailed comparison would require measurement of the transverse beam size as a function of time. This has not yet been undertaken.

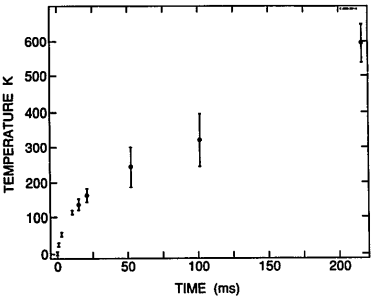

Fig. 5. Longitudinal temperature vs time after injection for $^7Li^+$ beam. A rapid heating of the longitudinal degree of freedom is observed, dominantly due to transverse to longitudinal coupling in the initially strongly coupled plasma.

The method of molecular dynamics [9] has also been applied to the problem of transverse to longitudinal energy transfer. The calculation starts with a system which has high kinetic energy in all three dimensions. When the system has equilibrated, the longitudinal motion is stopped. Following the reheating of the longitudinal degree of freedom then is analagous to the experiment represented in fig. 5. Computer size limitations prohibit simulating the actual particle density and transverse temperature corresponding to 10^9 particles in ASTRID. The calculations can, however, be employed to check the scaling relationships of the analytical model. For a system equivalent to 10^7 parti-

cles in ASTRID with transverse energies 0.3 to 2 meV, we obtain good agreement with the Sørensen method.

6. Laser cooling of metastable lithium

6.1. Fluorescence signal during the cooling process

Laser cooling of the metastable fraction of the lithium beam is achieved using two lasers. The co- and counterpropagating laser beams are carefully aligned to achieve maximum overlap with the circulating ions. At the time of injection, both lasers are on, with the copropagating laser initially in resonance with the slower ions. The couterpropagating laser is likewise initially in resonance with the faster ions. After injection, the frequency of the counterpropagating laser is swept towards higher frequencies. The light pressure force from the swept laser decelerates the ions to the velocities in resonance with the fixed-frequency laser, thereby reducing the velocity spread in the beam. Fig. 6 shows the fluorescent light produced in this process, plotted as a function of the frequency of the swept laser. This "cooling spectrum" is accumulated over many injection cycles of the machine in order to obtain good statistics.

The spectrum in fig. 6 exhibits some striking features. The sharp peak at the right side represents the fluorescence from the cooled velocity distribution as the swept laser decelerates the particles across the fixed laser. The detailed analysis of the cooling process, and determination of the temperature, appear below. The strong initial fluorescence, terminated by a sharp drop approximately 1 s after injection, is more difficult to account for. The position of the drop in the signal has been determined to be independent of the intensity, scanning rate, and detunings of the lasers. In addition, it is impossible to produce the cold distribution, identified by the sharp fluorescence peak, before the initial fluorescence has dropped off. These observations appear to indicate that whatever forces are active in the beam at early times they cannot be overcome by the laser cooling force. Without any competing heating mechanisms, the laser should be able to cool the metastable fraction to the Doppler limit in only 10 ms.

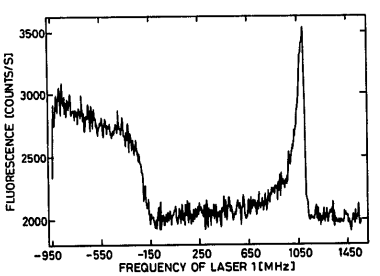

Fig. 6. Fluorescence vs laser frequency for the laser cooling process in $^7Li^+$. The sharp peak represents the laser-cooled ions. The longitudinal temperature of these cold ions is below 1 mK, corresponding to an energy spread of below 10^{-6}.

6.2. Measurement of the temperature

In order to measure the temperature of the cooled distribution, we use one laser as a probe. The intensity of the laser is lowered to minimize its perturbative effect on the velocity profile. Probe laser powers in the range of 10 to 100 times the saturation intensity of the transition were employed. We find that, for all powers used, the measured width of the distribution is equivalent to that one would expect from power broadening alone. Using the systematic errors in measuring the laser intensity and laser beam profile and the statistical errors, we can put an upper limit on the residual width due to Doppler (i.e. thermal) broadening. We obtain $T_{\|} \sim 1$ mK.

6.3. Calculation of the temperature

The velocity distribution of the cooled ions can be calculated from the velocity-dependent laser-induced force and diffusion. In the following we neglect intrabeam and other forces not related to the light force. We assume that at any instant the velocity distribution is stationary and determined by the actual laser field parameters. This assumption is supported by the experimental observation that, after the initial drop in fluorescence, the effectiveness of the cooling process is independent of the speed with which the frequency of the cooling laser is swept.

The velocity-dependent force is calculated by the continued fraction method [10]. The fluctuations in the light-induced force are described by a diffusion coefficient, derived using a procedure due to Minogin [11]. The velocity distribution for a given field configuration is obtained as a stationary solution to the Fokker–Planck equation. For the laser intensities and polarizations used in the ASTRID experiments, we obtain a minimum temperature of $T_{min} = 1$ mK.

7. Laser cooling and condensed beams

At the low temperatures attainable with laser cooling, the potential to achieve spatial ordering of the beam [12] exists. The simplest such condensed structure is a string of ions. For ASTRID, molecular dy-

namics simulations predict that 10^6 particles should condense into a string [13]. At higher densities the simulations predict the particles to condense into concentric shells. Presently, the prospects for creating a string of ions is investigated. To achieve order, the beam must be cold in all three degrees of freedom. The metastable fraction of the lithium beam amounts to about 10^5 particles, which is below the string threshold. The influence of the ground state ions, which are not subject to the laser cooling force, cannot be overlooked. It is difficult to imagine an ordered state coexisting with the warm ground state ions.

Also pertinent to the effort to obtain an ordered beam is our observation of strong forces which compete with the laser cooling process. The ability to laser cool the lithium ions is strictly correlated with the drop in fluorescence (fig. 6). This may indicate that a threshold phenomenon, like a beam instability, is active in the dense ASTRID beam. The inability of the laser to overcome the intrabeam forces may be due to the short range of the cooling force. The laser interacts only with those particles whose velocities lie within the power-broadened linewidth of the cooling transition. The vast majority of the particles are free to diffuse under the influence of other forces. The two-component nature of the lithium beam exacerbates this situation, since the ground state ions do not respond to the laser. Our experience suggests that further experimental efforts are necessary in order to understand the mechanisms which limit the effectiveness of the laser cooling force.

8. Isotopic and isobaric selectivity

A storage ring offers unique possibilities for ultra-high mass spectroscopy as well as isotopic and isobaric selectivity when combined with lasers.

One parameter is the ability to store energetic particles for extended times, allowing lasers to interact effectively with the stored ions. The interaction between light and matter offers several attractive features, of which one, laser cooling, has already been discussed. In addition to cooling, the light–matter interaction allows species in one specific quantum state, either electronic or nuclear, to be selectively accelerated and manipulated. Another feature in the light–matter interaction, implicitly assumed in laser cooling, is the high velocity/energy resolution, allowing accurate determinations of high voltages [14]. Finally, intense lasers induce strong nonlinear processes, like photodetachment and ionization. These processes allow stored ionic species to be selectively "destroyed".

This discussion can be exemplified by one case. We have successfully laser accelerated and cooled metastable lithium, while synchronously ramping the entire ASTRID lattice (dipole and quadrupole magnets), thus "eliminating" only the ground state lithium ions by dumping them on a beam scraper. This process is presently limited by the tunability of our dye lasers, allowing energy changes of $\sim 2\%$ at 100 kV.

9. Note

The "edge" phenomena have recently been further studied. It was found, that the prime reason for the sharp drop in fluorescence light during the laser cooling was a higher order vertical resonance in the beam, which showed up 1 s after injection and led to a substantial particle loss. By tuning the ring away from the design tune to a slightly different operating point, where no resonance occurred, the "edge" disappeared and laser cooling proceeded without complications. The final temperatures without the particle loss were significantly higher (200 mK). This is partly due to the extra diffusion of ions. A significant contribution might also come from another property of the resonance. It leads to cooling of the whole beam, which helps the laser cooling. This was found by laser spectroscopy of the beam with and without the resonance.

References

[1] S.P. Møller, ASTRID, a Storage Ring for Ions and Electrons, Proc. 14th Biennial Particle Accelerator Conf. San Francisco, USA, 1991, IEEE Catalog 91CH3038-7, p. 2811.
[2] M. Eriksson, Nucl. Instr. and Meth. A261 (1987) 39.
[3] J. Hangst, M. Kristensen J.S. Nielsen, O. Poulsen, J.P. Schiffer and P. Shi, Phys. Rev. Lett. 67 (1991) 1238.
[4] D.J. Wineland and H. Dehmelt, Bull. Am. Phys. Soc. 20 (1975) 637;
T. Hänch and A. Schawlow, Opt. Commun. 13 (1975) 68.
[5] S. Chu and C. Weiman, J. Opt. Soc. Am. B6 (1989) 2020.
[6] S. Schröder et al., Phys. Rev. Lett. 64 (1990) 2901, and private communication.
[7] J.P. Schiffer and P. Kienle, Z. Phys. A321 (1985) 181.
[8] A.H. Sørensen, in: CERN 87-10, ed. S. Turner (CERN, Geneva, 1987) pp. 135–154.
[9] A. Rahman and J.P. Schiffer, Phys. Rev. Lett. 57 (1986) 1133.
[10] V.G. Minogin and O.T. Serimaa, Opt. Commun. 30 (1979) 373.
[11] V.G. Minogin, Sov. Phys. JETP 53 (1981) 1164;
K. Berg-Sørensen et al., to be published.
[12] J.P. Schiffer and O. Poulsen, Europhys. Lett. 1 (1986) 55.
[13] A. Rahman and J.P. Schiffer, Phys. Scripta T22 (1988) 133.
[14] O. Poulsen and E. Riis, Metrologia 25 (1988) 147.